Particle-in-cell simulations of low-β magnetic reconnection driven by laser interaction with a capacitor–coil target

Xiaoxia Yuan(原晓霞)[1], Cangtao Zhou(周沧涛)[1,†], Hua Zhang(张华)[1,‡], Ran Li(李然)[1], Yongli Ping(平永利)[2], and Jiayong Zhong(仲佳勇)[2]

[1] *Shenzhen Key Laboratory of Ultraintense Laser and Advanced Material Technology, Center for Advanced Material Diagnostic Technology, and College of Engineering Physics, Shenzhen Technology University, Shenzhen* 518118, *China*

[2] *Department of Astronomy, Beijing Normal University, Beijing* 100875, *China*

(Received 22 December 2022; revised manuscript received 28 January 2023; accepted manuscript online 4 February 2023)

The dynamics of low-β magnetic reconnection (MR) driven by laser interaction with a capacitor–coil target are reexamined by simulations in this paper. We compare two cases MR and non-MR (also referred as AP-case and P-case standing for the anti-parallel and parallel magnetic field lines, respectively) to distinguish the different characteristics between them. We find that only in the AP-case the reconnection electric field shows up around the X line and the electron jet is directed toward the X line. The quadruple magnetic fields exist in both cases, however, they distribute in the current sheet area in the AP-case, and out of the squeezing area in the P-case, because electrons are demagnetized in the electron diffusion region in the MR process, which is absent in the P-case. The electron acceleration is dominant by the Fermi-like mechanism before the MR process, and by the reconnection electric field when the MR occurs. A power-law electron energy spectrum with an index of 1.8 is found in the AP-case. This work proves the significant potential of this experimental platform to be applied in the studies of low-β astronomy phenomena.

Keywords: magnetic reconnection, intense laser, low-β plasma

PACS: 41.75.Jv, 94.30.cp **DOI:** 10.1088/1674-1056/acb911

1. Introduction

Magnetic reconnection (MR) plays an important role in space and laboratory plasma by determining the topology of the magnetic field and releasing the energy stored in the magnetic field to plasma kinetic and thermal energies, such as in solar flares,[1–3] coronal mass ejections,[4,5] planetary magnetospheres,[6–9] and laboratory plasmas.[10] Since the concept of magnetic reconnection was first suggested by Giovanelli[11] about 70 years ago, it was widely used to explain explosive phenomena in space and laboratory plasma and has always been a hot topic.

In recent years, thanks to the rapid development of high power-laser technology, magnetic reconnection experiments in laser-driven high-energy-density (HED) plasmas have been extensively performed on different laser facilities, including OMEGA,[12] Vulcan,[13] and Shenguang-II.[14] In these experiments, the magnetic field configuration is built on the Biermann battery mechanism through the laser-target interaction process, the generated side-by-side plasma bubbles usually go through colliding, squeezing, and reconnecting three steps. Alternatively, insert external magnetic fields generated by external currents in two laser-generated plasma bubbles to perform MR. Magnetic field annihilation and outflow jets discovered in these experiments are regarded as evidences of MR.[15] However, the flow-driven MR with the high thermal pressure, $\beta = p_e/(B^2/2\mu_0) > 1$, in these cases is less relevant to most astronomy phenomena. Experiments on MR have also been conducted on large dedicated plasma devices, such as the MRX,[16] VTF,[17] and Keda linear magnetized plasma device,[18] *etc*. The fundamental physical processes of magnetic reconnection are further revealed, including testing the Sweet–Parker MHD model,[19] identifying the ion diffusion,[20] and electron diffusion[21] regions. In these experiments, the plasma β is less than 1, *i.e*., MR process is dominant by magnetic pressure, which is similar to the corona and chromosphere plasma.[22] More recently, kinetic simulations have revealed that MR leads to nonthermal electron acceleration and forms a power-law distribution in the low-β regime, but not in the high-β regime.[23]

A robust low-β experiment platform using high-power lasers interacting with a double capacitor–coil target composed of two metal coils connecting two metal foils draws more and more attention recently. The first experiment was conducted using one coil getting 60 T by Daido *et al*. in 1986,[24] further contributions were made by different groups and until now up to kiloTesla magnetic field has been achieved.[25,26] With the double-coil target, two parallel coil currents are driven by the electric potential between the two target foils generating toroidal magnetic fields, which are antiparallel between the coils allowing MR occurs there. Pei

[†]Corresponding author. E-mail: zhoucangtao@sztu.edu.cn
[‡]Corresponding author. E-mail: zhanghua@sztu.edu.cn

© 2023 Chinese Physical Society and IOP Publishing Ltd

et al.[27] first demonstrated the feasibility of studying low-β MR using this platform on GEKKO-XII laser facility and obtained the $\beta \sim 0.016$. Thanks to this experiment configuration, the direct measurement of the nonthermal electrons from MR becomes feasible,[28] which is limited in the dedicated devices like MRX, because of the larger system size compared to the short mean free path and Debye lengths. Experiments[27,29] and kinetic simulations[30,31] depend on this configuration have revealed MR outflow, quadruple magnetic fields, and nonthermal electron acceleration. Different acceleration mechanisms have been studied theoretically and numerically, including direct acceleration of reconnection electric field where the particles drift along the reconnection electric field following the Speiser orbits,[32–34] Fermi mechanism that is the particles are reflected in contract magnetic island[35,36] or by the moving magnetic field lines[37,38] and gain kinetic energy, betatron acceleration that is the magnetized electron is accelerated by the perpendicular inductive electric field generated by the enhancement magnetic field,[39–41] and parallel electric field acceleration along the magnetic fields.[42–44]

In this paper, we perform two-dimensional (2D) PIC simulations to examine MR and non-MR dynamics based on the experimental configuration by Pei *et al.*[27] We consider two cases, the magnetic fields generated in the middle region by two driving currents are antiparallel and parallel, referred to as AP-case and P-case, respectively, and naturally, there is no reconnection in the latter case. In the paper of Huang *et al.*,[30] the simulation of the AP-case has been performed and found that the electrons are accelerated forming a power-law with an index of 3. We compare the AP-case and P-case and find that they both experience expanding and squeezing phases until the AP-case comes to the reconnection stage, and the P-case still squeezes. In the early stage, the electrons are heated in the same way by the Fermi-like acceleration mechanism in both cases, and in the later stage the reconnection dominates the acceleration process in the AP-case, and forms a power-law distribution with an index of 1.8 based on our parameters. The comparisons distinguish the features of the AP-case and P-case, which will help us to understand low-β phenomena in astrophysics and guide future laser-driven capacitor–coil experiments.

The experimental scheme and the simulation setup are described in Section 2, the simulation results are presented in Section3, Sections 4 and 5 give discussion and conclusion, respectively.

2. Experimental setup and simulation model

Figure 1(a) shows the experimental scheme of low-β magnetic reconnection. The capacitor–coil target is composed of two nickel disks connecting with two nickel U-shaped parallel-placed coils, the separation of the disks is $\sim$ 600 μm, as well as the separation of the coils. The radius of the coil-bend and the length of the straight part of the coil are $\sim$ 300 μm and $\sim$ 600 μm, respectively. The cross-section of the coil is $\sim$ 100 μm $\times$ 100 μm. The long pulse laser beams go through the entrance hole (with a diameter of $\sim$ 1600 μm) in the front disk and interact with the rear disk generating electric potential which induces intense driving currents in the coils. Figure 1(c) shows the target of the P-case, where the U-turn coil currents are antiparallel for which longer coils are used. Figures 1(b) and 1(d) show the zoomed-in U-turn coils along with the coil currents, and the reconnection/squeezing planes which are the simulation domains cross the tips of the coils. The sampled magnetic field lines show the "push" reconnection magnetic geometry, *i.e.*, the currents increase rapidly inducing the expansion of the magnetic fields during this phase in Fig. 1(b), and squeezing magnetic geometry in Fig. 1(d).

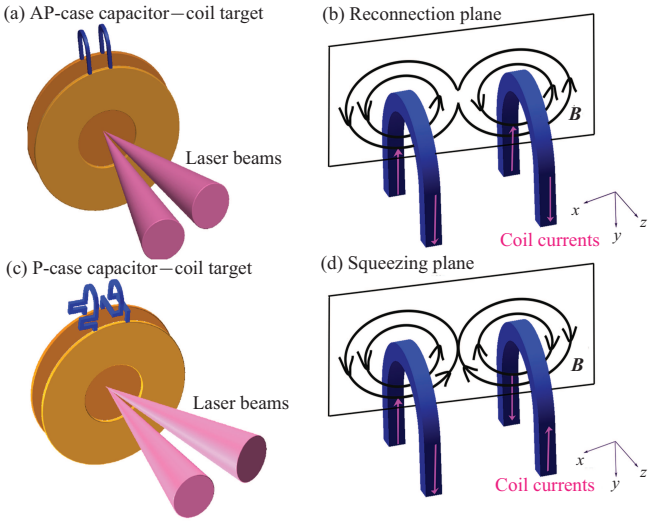


Fig. 1. Schematics of the experimental setup of the laser-driven capacitor–coil target in (a) the AP-case and (c) the P-case. (b) and (d) Zoomed-in coil along with the square line box (reconnection/squeezing plane) where is the 2D simulation domain. The black curve lines with the arrows are the sampled magnetic field lines showing the reconnection/squeezing geometry, only the U-turn part is shown in panel (d).

We now consider the reconnection simulation in the (x,y) coordinates using EPOCH PIC code, which uses finite-difference time-domain method for solving Maxwell's equations and particle pusher solves the relativistic equation of motion under the Lorentz force for each particle.[45] An initial uniform background plasma with the electron density of $n_{e0} = 1\times10^{18}$ cm^{-3} and ion density of $n_{i0} = 0.17\times10^{18}$ cm^{-3} are set, because the laser–target interaction process which is the source of background plasma in the experiment is not included in the simulations. Assuming the coil currents increase linearly during the laser duration and decay exponentially after the laser off, the peak current is 45 kA and defined on the grids in the PIC code, the magnetic fields are generated self-consistently by solving Maxwell's equations. The raising time $t_r = 2\Omega_{i0}^{-1}$, where $\Omega_{i0}^{-1} = m_i/ZeB_0$ is the ion gyrocycle, $Z = 6$ and the decay time $t_d = 7\Omega_{i0}^{-1}$ (based on the decay time of L/R).[46] The simulation parameters are similar with the experiments conducted by Pei *et al.*[27] The particle temperature is $T_e = T_i = 100$ eV, and the peak magnetic field B_0 at the midpoint of the line connecting the two coil-bend centers is ~ 59 T, $\beta = p_e/(B^2/2\mu_0) = n_e kT_e/(B^2/2\mu_0) = 0.012$.

The simulation rectangular domain is $[-L_x, L_x]$ and $[-L_y, L_y]$, $L_x = L_y = 2d_i$, d_i is the ion inertial length. The grid number is $N_x \times N_y = 1000\times1000$, the size of the grid is $\Delta x = \Delta y \sim 2.8$ μm, cells are typically of the scale of the Debye length. Each grid includes 200 particles per species. The ion-to-electron mass ratio $m_i/Zm_e = 100$ and the light speed is $c = 20V_A$, V_A is the Alfvén speed which is based on B_0 and n_{e0}. The system adopts the open and conduct boundaries for particle and electromagnetic fields, respectively. The magnetic field is normalized by B_0. A summary of the parameters in the simulation is given in Table 1.

Table 1. Physical parameters in the PIC simulations. m_p is the proton mass.

Parameter	Estimated values
Ion (Ni) mass m_i	$58.6934m_p$
Ion charge Z	6
Electron density n_{e0}	1.0×10^{18} cm^{-3}
Ion density n_{i0}	0.17×10^{18} cm^{-3}
Electron and ion temperature T	100 eV
Magnetic field B_0	59 T
Radius of the coils R	300 μm
Coil separation distance D	600 μm
Ion inertial length d_i	705 μm
Ion gyrofrequency Ω_{i0}	0.6×10^9/s
Alfven speed V_A	405 km/s
Plasma β	~ 0.012

Two different cases are considered for comparison in this paper, one is the reconnection case with the parallel driving currents in the z direction, MR occurs in the middle zone, which is referred to AP-case. In contrast, the non-reconnection case (P-case) has antiparallel driving currents.

3. Simulation results

Firstly, we reexamine the dynamics of the MR process in the AP-case, figure 2 shows the evolutions of the magnetic field B/B_0 and current density $J_z/en_{e0}V_A$ at $\Omega_{i0}t = 0.5, 1.2, 2.2$, and 2.5. As the driving currents rise, the magnetic bubbles expand pushing the initial plasma outwards, and out-of-plane currents J_z are generated by $J = \nabla\times B/\mu_0$ at the edge of the magnetic bubbles. When the two magnetic bubbles collide and squeeze with each other, a current sheet forms in the middle of the two bubbles. When the width of the current sheet becomes thin enough, $\sim 0.2d_i$, magnetic reconnection occurs, and a single X line forms in the current sheet. With the proceeding of the MR, the current sheet tears up and becomes expanding. The reconnection process lasts about $0.7\Omega_{i0}^{-1}$. Based on the evolution of the current sheet, the whole process in the AP-case can be divided into four phases, the magnetic bubbles expand roughly at $\Omega_{i0}t = 0.0 \sim 1.0$, collide and squeeze at $\Omega_{i0}t = 1.0 \sim 1.6$, reconnect at $\Omega_{i0}t = 1.6 \sim 2.3$, and end after $\Omega_{i0}t = 2.3$ in the AP-case.

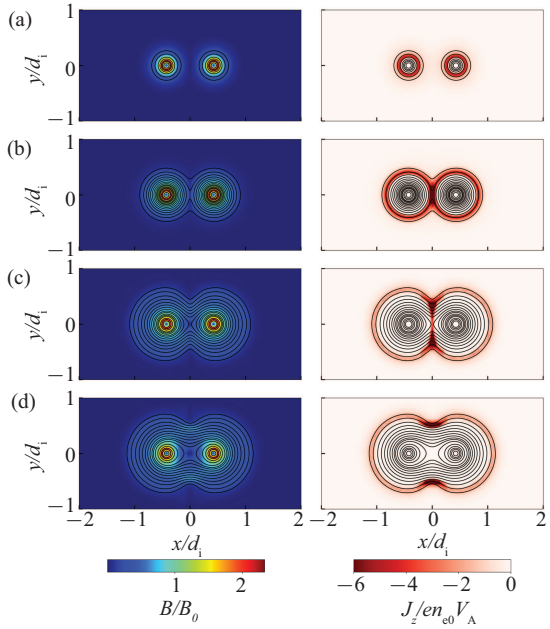


Fig. 2. The magnetic field B/B_0 and the current density $J_z/en_{e0}V_A$ at (a) $\Omega_{i0}t = 0.5$, (b) $\Omega_{i0}t = 1.2$, (c) $\Omega_{i0}t = 2.2$, and (d) $\Omega_{i0}t = 2.5$ in the AP-case. The black in-plane magnetic field lines are also plotted in the figures for reference.

Figure 3 shows the time evolutions of the reconnected magnetic flux $\Phi_B/B_0d_i = \int B\times dl/B_0d_i$, where dl is the line element of the integration path ($y = -2 \sim 2d_i$, $x = 0$), and the reconnection rate $\partial\Phi_B/\partial t$ in the AP-case and P-case. The reconnection rate reaches the max at $\Omega_{i0}t = 2.3$. However, it

is clear that there is no reconnection takes place in the P-case, only squeezing and magnetic field enforcement occur between the bubbles, thus the reconnection rate and the reconnected flux are nearly 0 during the whole time.

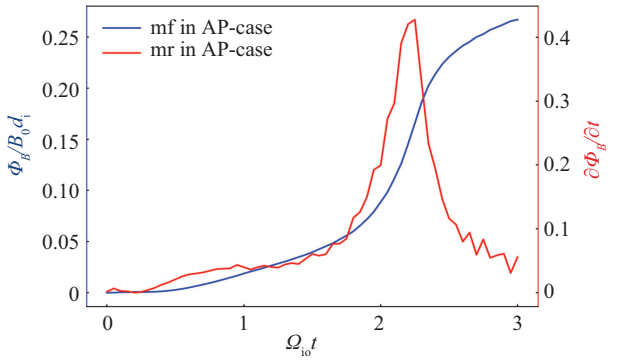


Fig. 3. The time evolutions of the reconnected magnetic flux (mf) Φ_B/B_0d_i and the magnetic reconnection rate (mr) $\partial\Phi_B/\partial t$ in the AP-case.

In order to distinguish the different characters between the AP-case and P-case, we compare a set of quantities including the magnetic field B/B_0, out-of-plane electric field E_z/V_AB_0, out-of-plane magnetic field B_z/B_0, current density in the y direction $J_y/en_{e0}V_A$, and temperature T_e/T_0 at two different times $\Omega_{i0}t = 1.2$ and 2.2, respectively, as shown in Figs. 4 and 5.

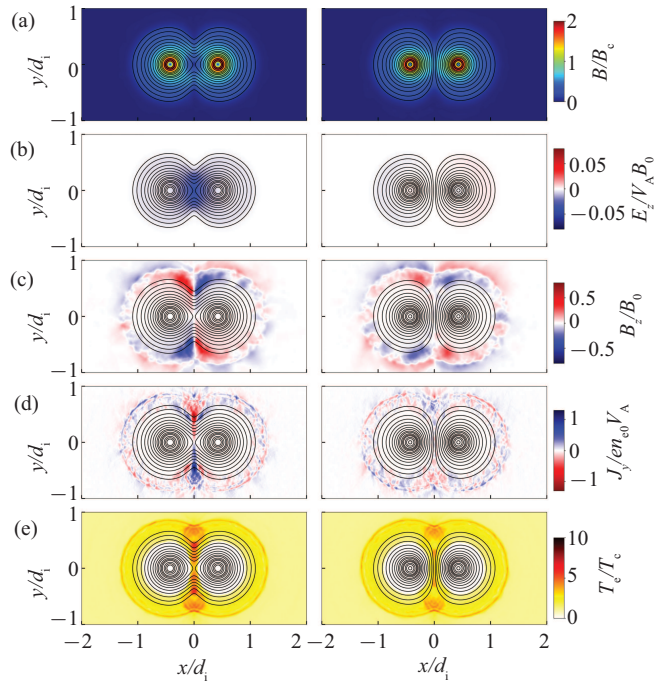


Fig. 4. Comparisons between the AP-case (left column) and the P-case (right column) at the squeezing stage at $\Omega_{i0}t = 1.2$ for (a) magnetic field B/B_0, (b) electric field in the z direction E_z/V_AB_0, (c) out-of-plane magnetic field B_z/B_0, (d) current density in the y direction $J_{ey}/en_{e0}V_A$, and (e) electron temperature T_e/T_0. The black in-plane magnetic field lines are also plotted in the figures for reference.

At the time of $\Omega_{i0}t = 1.2$, *i.e.*, the squeezing phase, all the qualities in both cases are very similar. We can see that the electrons are heated because of the resulting motional electric field when they are reflected between the magnetic bubbles, which is known as the Fermi-like mechanism. At the time of $\Omega_{i0}t = 2.2$, the X-type reconnection is taking place in the AP-case, and an out-of-plane electric field is generated around the X line. In contrast, the magnetic bubbles are still squeezed by each other enforcing the magnetic field strength, and the out-of-plane electric fields between the bubbles are cancelled out by each other in the P-case. The out-of-plane electric fields in the bubbles are induced by $-v \times B$, where v is the velocity of the magnetic lines. The magnetic bubbles expands/contracts because of the increasing/decreasing of the driving currents, which results the different directions in the out-of-plane electric fields in the bubbles.

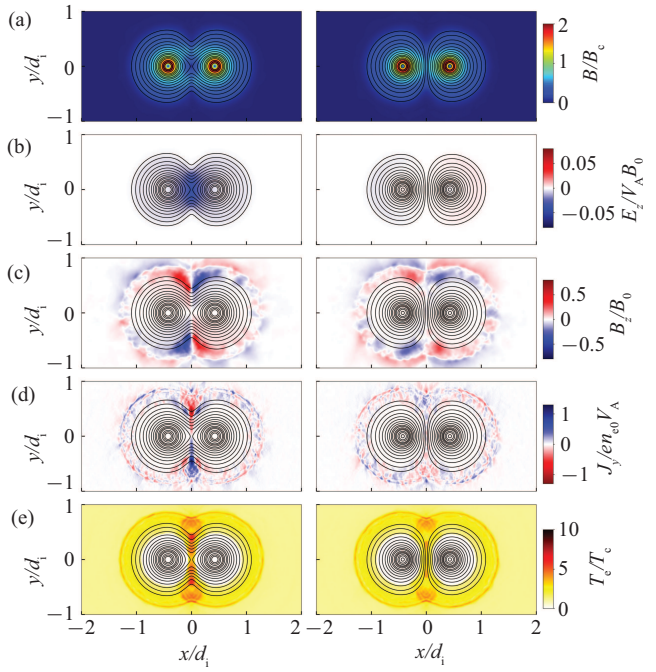


Fig. 5. Comparisons between the AP-case (left column) and the P-case (right column) at $\Omega_{i0}t = 2.2$ for (a) magnetic field B/B_0, (b) electric field in the z direction E_z/V_AB_0, (c) out-of-plane magnetic field B_z/B_0, (d) current density in the y direction $J_y/en_{e0}V_A$, and (e) electron temperature T_e/T_0. The black in-plane magnetic field lines are also plotted in the figures for reference.

In Fig. 5(c), the quadruple magnetic fields show up in both cases. From the time evolution of the simulations, the quadruple fields become more and more intense after the MR takes place, and distribute in the current sheet area in the AP-case. In the P-case, the quadruple fields are less intense and only distribute out of the squeezing area. The ions between the two bubbles are easily demagnetized when two bubbles collide in both cases, due to the large mass. However, the electrons are magnetized all the time except in the electron diffusion region in the reconnection case. Thus, the electrons are decoupled with the magnetic field lines in the current sheet in the AP-case, and the outflow electrons cause stronger net electron currents, which induce stronger quadruple fields. Although the quadruple fields can not be treated as the direct

criterion of MR, the observation of quadruple fields in the collisionless regime indicates Hall effects, which have been verified to speed up the reconnection rate.[47] Another important characteristic of magnetic reconnection is electron outflow indicated by current density J_{ey}, which is directed to the X line in the outflow regions and be outside the peaks of the quadruple fields[48] in the AP-case. The reason for the formation of J_{ey} is the rapid movement of the magnetic field lines away from the current sheet, and the electrons in the outflow regions are continuously bounced.[30] Electron outflow has been verified as a criterion for reconnection in both simulations and experiments.[49,50] There is no current density in the P-case where no MR occurs. The fluctuations with alternate positive and negative values at the edge of the magnetic bubbles shown in Figs. 4(c), 4(d) and 5(c), 5(d) are probably caused by Weibel instability which is similar to the process found in Ref. [39].

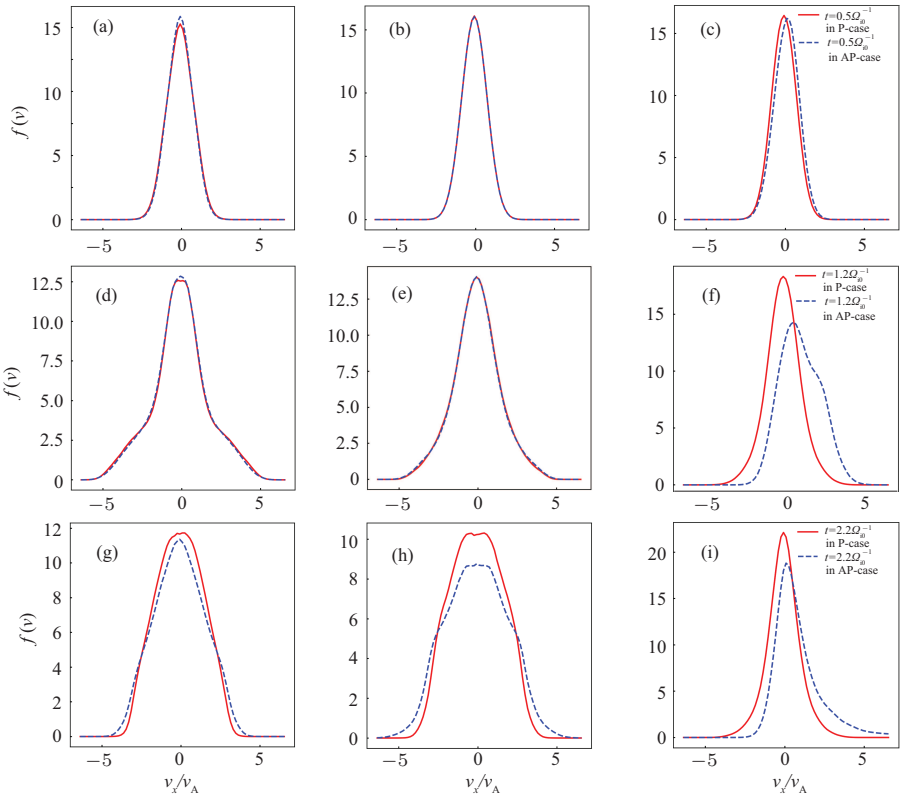


Fig. 6. The velocity distributions (v_x, v_y, v_z) of the electrons at the location of $x = -0.1 \sim 0.1d_i$, $y = -1.0 \sim 1.0d_i$ for the AP-case and P case at (a)–(c) $\Omega_{i0}t = 0.5$, (d)–(f) $\Omega_{i0}t = 1.2$, and (g)–(i) $\Omega_{i0}t = 2.2$.

In Fig. 5(e), we can see that the electron temperature in the current sheet is higher in the AP-case than P-case, which is because the electrons are heated mainly by the Fermi-like mechanism in the P-case. However, in the AP-case reconnection electric field makes an additional contribution. Figure 6 shows the distributions of the electron velocities v_x, v_y, and v_z at $\Omega_{i0}t = 0.5$, $\Omega_{i0}t = 1.2$, and $\Omega_{i0}t = 2.2$ at the location of $x = -0.1 \sim 0.1d_i$ and $y = -1.0 \sim 1.0d_i$. At $\Omega_{i0}t = 0.5$, we can see that the velocity distributions in three different directions are overlapped with each other in both cases, and obey Gaussian distribution because at the early expanding stage electrons are barely heated. As the magnetic bubbles squeeze each other, they are mainly heated by the Fermi-like mechanism in both cases as mentioned before, as shown in Figs. 6(d), 6(e), and 6(f). Note that v_z distribution is different in the AP-case and P-case, as shown in Fig. 6(f), because of the different electrons movements. The electrons are energized by the resulting motional electric field when they bounce between the bubbles, as shown in Figs. 7(a) and 7(b). The electrons obtain a net movement in the z direction in the AP-case, as shown in Figs. 7(c), 7(e), and 7(g), the velocity v_z is positive all the time. However, the electrons oscillate back and forth in the z direction in the P-case, as shown in Figs. 7(d), 7(f), and 7(h), and the velocity alternates between negative and positive, this is similar to the process studied in Ref. [37]. The small circles show the picks of v_z and the corresponding positions. Based on the knowledge of electron movement in the magnetic field we know that the v_z in Figs. 7(c), 7(e), and 7(g) decreases after the rebounded by the magnetic field lines, because part of the velocity converts to v_x during the electron gyromotion, and in Figs. 7(d), 7(f), and 7(h) the velocity changes between positive and negative, because the electron moves in the opposite directional magnetic fields. As the reconnection proceeds, the electrons flow out of the current sheet region and are heated in the y direction. The out-of-plane electric field around the X line generated during the reconnection process accelerates electrons causing a

tail in the AP-case, as shown in Fig. 6(i). Figures 8(a), 8(c) and 8(b), 8(d) show the typical electron trajectories in the AP-case and P-case during $\Omega_{i0}t = 1.2 \sim 2.2$. Figure 8(e) shows the tracked electron energy *versus* time. The electron energy increases fast after arriving at the out-of-plane electric field in the AP-case. In the P-case, there is no reconnection electric field generated, only electron bouncing between the magnetic field lines, thus the electron gains little energy, which confirms the contribution to the electric acceleration from the reconnection electric field during the MR process.

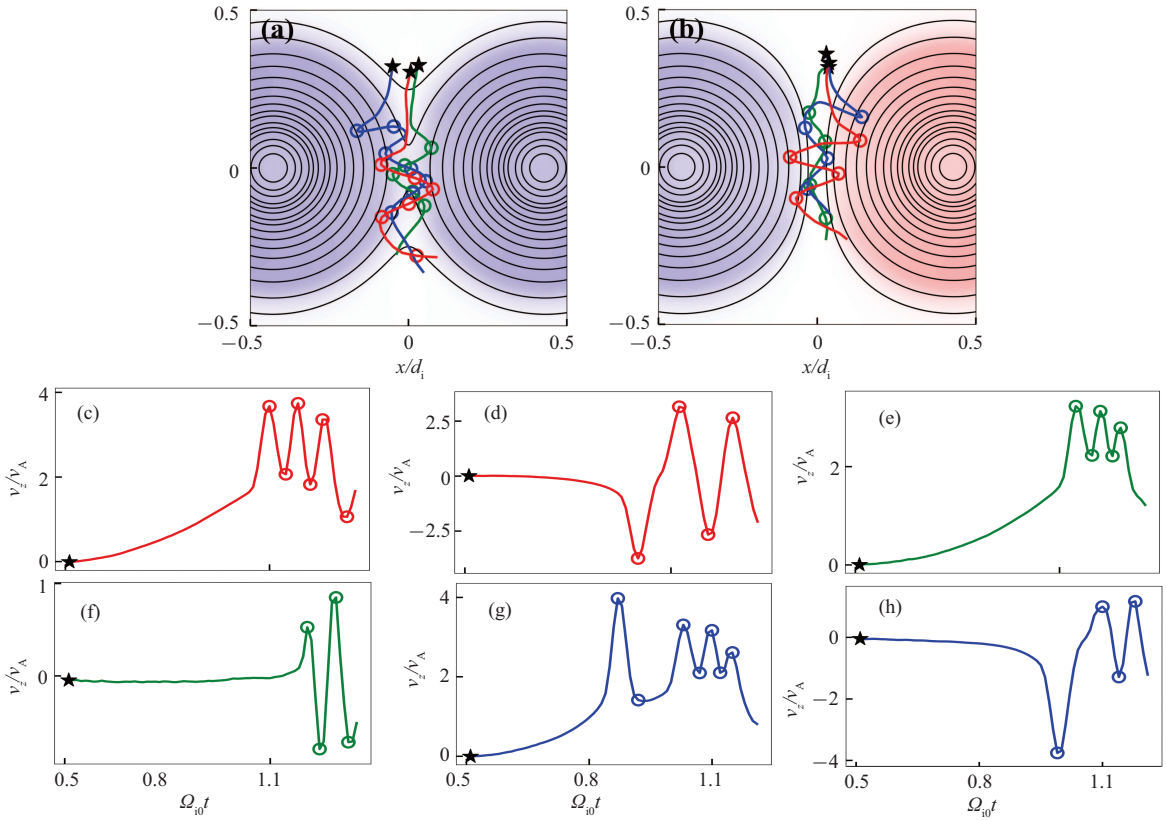


Fig. 7. Typical trajectories of three thermal electrons during $\Omega_{i0}t = 0.5 \sim 1.2$ in (a) the AP-case and (b) the P-case, and the magnetic field lines and the out-of-plane electric field at $\Omega_{i0}t = 1.2$ are plotted for reference. (c)–(h) The electron velocity v_z *versus* time of the tracked electrons in panels (a) and (b). The small circles represent the picks of v_z of the tracked electrons in panels (c) and (d), the corresponding positions in panels (a) and (b), respectively. The black star represents $\Omega_{i0}t = 0.5$.

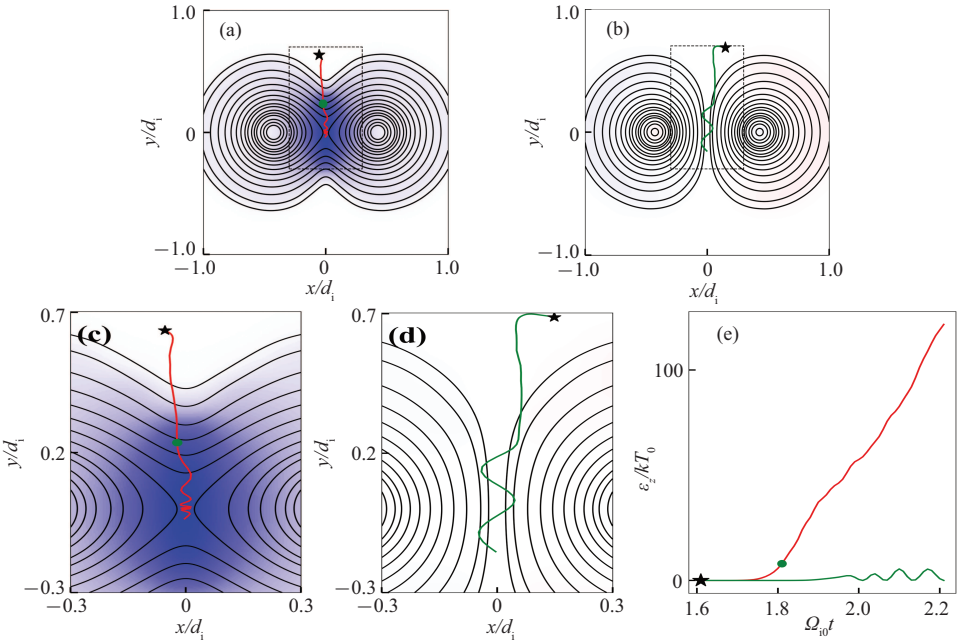


Fig. 8. Typical trajectories of nonthermal and thermal electrons during $\Omega_{i0}t = 1.6 \sim 2.2$ in (a) the AP-case and (b) the P-case, respectively, and the magnetic field lines and the out-of-plane electric field at $\Omega_{i0}t = 2.2$ are plotted for reference. Panels (c) and (d) show the zoomed views of the dashed black squares in panels (a) and (b). (e) The red and green lines are the electron energy *versus* time for the tracked electrons in panels (a) and (c), and panels (b) and (d). The black star and green dot represents $\Omega_{i0}t = 1.6$ and 1.8, respectively.

Figure 9(a) shows the electron energy spectra counting the electrons at $\Omega_{i0}t = 0.5$, $\Omega_{i0}t = 1.2$, and $\Omega_{i0}t = 2.2$ at the location of $x = -0.1d_i \sim 0.1d_i$ and $y = -1.0d_i \sim 1.0d_i$ in the AP-case and the P-case. The population of the energetic electrons becomes larger and larger with the MR proceeding in the AP-case as shown in Fig. 9(b) and forms a power-law distribution with an index of 1.8 at $\Omega_{i0}t = 2.2$. For the P-case, the electron energy spectrum at $\Omega_{i0}t = 1.2$ includes more energetic electrons than $\Omega_{i0}t = 0.5$ because of the Fermi-like accelerated, and also more than that at $\Omega_{i0}t = 2.2$, which is due to part of the electrons flowing out of the counting zone with the time evolution. Therefore, here we can conclude that the reconnection electric field dominates the electron acceleration of the power-law distribution, not the Fermi-like mechanism.

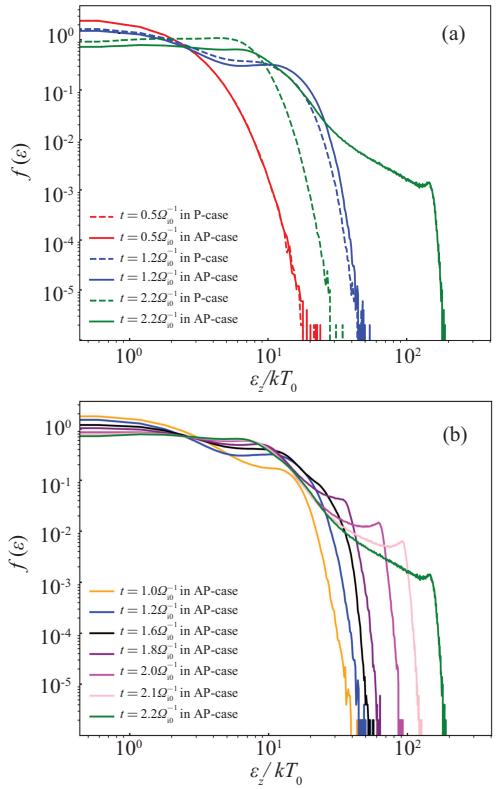


Fig. 9. (a) The electron energy spectrum for the AP case and the P-case at $\Omega_{i0}t = 0.5$, 1.2, and 2.2, respectively; (b) the electron energy spectrum for the AP-case at $\Omega_{i0}t = 1.0$, 1.2, 1.6, 1.8, 2.0, 2.1, and 2.2, at the location of $x = -0.1d_i \sim 0.1d_i$, $y = -1.0d_i \sim 1.0d_i$.

4. Discussion

Laser interacting with a double capacitor–coil target is proved to generate up to kiloTesla magnetic field.[25,51] Such a strong external magnetic field has broad potential applications to many subjects besides magnetic reconnection, such as guiding and controlling charged particle,[52] plasma magnetohydrodynamics study,[53] relaxing the requirements for fusion ignition,[54,55] generation of high-power circularly-polarized laser pulses,[56] mitigation of stimulated Raman scattering instability in ICF[57] or laser amplification via magnetized low-frequency scattering,[58] *etc*.

The acceleration mechanisms of the nonthermal electron and the formation of a power-law spectrum have been central topics in magnetic reconnection studies. Fermi-like and reconnection electric field mechanisms both are proved to play essential roles in energizing particles and forming a power-law spectrum.[36,59–61] In this paper, we address the acceleration of the nonthermal electrons is dominated by the electric field generated in the reconnection of the laser interaction with the capacitor–target, excluding the effect of the Fermi-like mechanism. However, for the MR in the HEDP regime, where two interaction plasma bubbles are generated by laser irradiating a plane target, the reconnection is mainly flow-driven and β is always larger than 1,[50] the Fermi-like acceleration is also important for the generation of energized electrons. Because this regime always leads to a higher initial electron energy which causes a stronger Fermi effect than ours which is low β and magnetically driven.[37] There are studies arguing that some loss mechanism is needed to balance the energy gain for forming a power-law distribution in a system.[59–61] The simplified power-law spectral index model is $\sim 1+(\alpha\tau_{\rm esc})^{-1}$, where $\alpha = {\rm d}\varepsilon/{\rm d}t * \varepsilon^{-1}$ is the acceleration rate, where ε is the particle energy, $\tau_{\rm esc} \sim L/V_{\rm A}$ is the escape time, L is the characteristic length, $V_{\rm A}$ is the Alfvén speed.[59] Alfvén speed characterizes the outflow speed which affects the energy loss when particles flow out of the system.

5. Conclusions

In this paper, we perform 2D PIC simulations for studying dynamics of MR and non-MR, respectively, based on laser-driven capacitor target. Through the comparisons, we find that the quadruple fields exist in both cases, however, in the AP-case electrons are demagnetized in the electron dissipation layer causing stronger quadruple fields in the current sheet area, and in the P-case the quadruple fields are at the area out of the squeezing region. The electrons outflow is believed as an important feature for MR, and cannot be obviously found in the P-case. During the squeezing stage, electrons are mainly accelerated by Fermi-like mechanism, the reconnection electric field dominates the nonthermal acceleration with the MR proceeding and forms a power-law spectrum with an index of 1.8. The experimental setup we proposed provides more possibilities to study the similar low-β magnetic reconnection in astronomy.

Acknowledgement

Project supported by the National Natural Science Foundation of China (Grant No. 11875092).

References

[1] Parker E N 1957 *J. Geophys. Res.* **62** 509

[2] Parker E N 1963 *Astrophys. J. Suppl. Ser.* **8** 177
[3] Shibata K and Magara T 2011 *Living Rev. Sol. Phys.* **8** 1
[4] Antiochos S K, DeVore C R and Klimchuk J A 1999 *Astrophys. J.* **510** 485
[5] Cassak P A, Mullan D J and Shay M A 2008 *Astrophys. J.* **676** 2008
[6] Angelopoulos V, McFaddenJ P, Larson D, Carlson C W, Mende S B, Frey H, Phan T, Sibeck D G, Glassmeier K H, Auster U, Donovan E, Mann I R, Rae I J, Russell C T, Runov A, Zhou X Z and Kepko Larry 2008 *Science* **321** 931
[7] Nagai T, Fujimoto M, Saito Y, Machida S, Terasawa T, Nakamura R, Yamamoto T, Mukai T, Nishida A and Kokubun S 1998 *J. Geophys. Res. Space Phys.* **103** 4419
[8] Lu Q M, Fu H S, Wang R S and Lu S 2022 *Chin. Phys. B* **31** 089401
[9] Zhang T L, Lu Q M, Baumjohann W, Russell CT, Fedorov A, Barabash S, Coates A J, Du A M, Cao J B, Nakamura R, Teh W L, Wang R S, Dou X K, Wang S, Glassmeier K H, Auster H U and Balikhin M 2022 *Chin. Phys. B* **31** 089401
[10] Wesson J A 1990 *Nucl. Fusion* **30** 2545
[11] Giovanelli R 1946 *Nature* **158** 81
[12] Li C K, Séguin F H, Frenje J A, Rygg J R, Petrasso R D, Town R P J, Amendt P A, Hatchett S P, Landen O L, Mackinnon A J, Patel P K, Tabak M, Knauer J P, Sangster T C and Smalyuk V A 2007 *Phys. Rev. Lett.* **99** 015001
[13] Nilson P M, Willingale L, Kaluza M C, Kamperidis C, Minardi S M, Wei S, Fernandes P, Notley M, Bandyopadhyay S, Sherlock M, Kingham R J, Tatarakis M, Najmudin Z, Rozmus W R, Evans G M, Haines G A, Dangor E and Krushelnick K 2006 *Phys. Rev. Lett.* **97** 255001
[14] Zhong J Y, Li Y T, Wang W G , Wang J Q, Dong Q L, Xiao C J, Wang S J, Liu X, Zhang L, An L, Wang F L, Zhu J Q, Gu Y, He X T, Zhao G and Zhang J 2010 *Nat. Phys.* **6** 984
[15] Fiksel G, Fox W, Bhattacharjee A, Barnak D, Chang P Y, Germaschewski K, Hu S and Nilson P 2014 *Phys. Rev. Lett.* **113** 105003
[16] Yamada M, Ji H, Hsu S, Carter T, Kulsrud R, Ono Y and Perkins F 1997 *Phys. Rev. Lett.* **78** 1997
[17] Egedal J, Fox W, Katz N, Porkolab M, Reim K and Zhang E 2007 *Phys. Rev. Lett.* **98** 015003
[18] Sang L, Lu Q, Xie J, Fan F, Zhang Q, Ding W, Zheng J and Sun X 2022 *Phys. Plasmas* **29** 102108
[19] Ji H, Yamada M, Hsu S and Kulsrud R 1998 *Phys. Rev. Lett.* **80** 3256
[20] Ren Y, Yamada M, Gerhardt S, Ji H, Kulsrud R and Kuritsyn A 2005 *Phys. Rev. Lett.* **95** 055003
[21] Ren Y, Yamada M, Ji H P, Gerhardt S P and Kulsrud R 2008 *Phys. Rev. Lett.* **101** 085003
[22] Gary G A 2001 *Sol. Phys.* **203** 71
[23] Guo F, Li H, Daughton W and Liu Y H 2014 *Phys. Rev. Lett.* **113** 155005
[24] Daido H, Miki F, Mima K, Fujita M, Sawai K, Fujita H, Kitagawa Y, Nakai S and Yamanaka C 1986 *Phys. Rev. Lett.* **56** 846
[25] Santos J, Bailly-Grandvaux M, Giuffrida L, *et al*. 2015 *New J. Phys.* **17** 083051
[26] Fujioka S, Zhang Z, Ishihara K, Shigemori K, Hironaka Y, Johzaki T, Sunahara A, Yamamoto N, Nakashima H, Watanabe T, Shiraga H, Nishimura H and Azechi H 2013 *Sci. Rep.* **3** 1170
[27] Pei X X, Zhong J Y, Sakawa Y, Zhang Z, Zhang K, Wei H G, Li Y T, Li Y F, Zhu B J, Sano T, Hara Y, Kondo S, Fujioka S, Liang G Y, Wang F L and Zhao G 2016 *Phys. Plasmas* **23** 032125
[28] Chien A, Gao L, Zhang S, *et al*. arXiv: 2201.10052 physics.plasm-ph
[29] Yuan X X, Zhong J Y, Zhang Z, *et al.* 2018 *Plasma Physics and Controlled Fusion* **60** 065009
[30] Huang K, Lu Q, Gao L, Ji H T, Wang X and Fan F 2018 *Phys. Plasmas* **25** 052104
[31] Huang K, Lu Q, Chien A, Gao L, Ji H T, Wang X and Wang S 2020 *Plasma Physics and Controlled Fusion* **63** 015010
[32] Cerutti B, Werner G R, Uzdensky D A and Begelman M C 2013 *Astrophys. J.* **770** 147
[33] Speiser T 1965 *J. Geophys. Res.* **70** 4219
[34] Huang C, Lu Q and Wang S 2010 *Phys. Plasmas* **17** 072306
[35] Drake J, Swisdak M, Che H and Shay M 2006 *Nature* **443** 553
[36] Fu X R, Lu Q M and Wang S 2006 *Phys. Plasmas* **13** 012309
[37] Huang K, Lu Q M, Huang C, Dong Q L, Wang H Y, Fan F B, Sheng Z M, Wang W and Zhang J 2017 *Phys. Plasmas* **24** 102101
[38] Totorica S R, Abel T and Fiuza F 2016 *Phys. Rev. Lett* **116** 095003
[39] Lu S, Lu Q M, Guo F, Sheng Z M, Wang H Y and Wang S 2016 *New J. Phys.* **18** 013051
[40] Hoshino M, Mukai T, Terasawa T and Shinohara I 2001 *J. Geophys. Res. Space Phys.* **106** 25979
[41] Huang C, Wu M, Lu Q, Wang R and Wang S 2015 *J. Geophys. Res. Space Phys.* **120** 1759
[42] Egedal J, Daughton W and Le A 2012 *Nat. Phys.* **8** 321
[43] Drake J F, Shay M A, Thongthai W and Swisdak M 2005 *Phys. Rev. Lett* **94** 095001
[44] Nan J, Huang K, Lu Q, Lu S, Wang R, Xie J and Zheng J 2022 *J. Geophys. Res. Space Phys.* **127** e2021JA029996
[45] Arber T, Bennett K, Brady C, Lawrence-Douglas A, Ramsay M, Sircombe N, Gillies P, Evans R, Schmitz H, Bell A and Ridgers C 2015 *Plasma Physics and Controlled Fusion* **57** 113001
[46] Chien A, Gao L, Ji H T, Yuan X X, Blackman E G, Chen H, Efthimion P C, Fiksel G, Froula D H, Hill K W, Huang K, LU Q M, Moody J D and Nilson P M 2019 *Phys. Plasmas* **26** 062113
[47] Ji H T, Terry S, Yamada M, Kulsrud R, Kuritsyn A and Ren Y 2004 *Phys. Rev. Lett.* **92** 115001
[48] Lu Q, Huang C, Xie J, Wang R, Wu M, Vaivads A and Wang S 2010 *J. Geophys.* **115** A11208
[49] Dong L Q, Wang S J, Lu Q M, *et al.* 2012 *Phys. Rev. Lett.* **108** 215001
[50] Huang K, Huang C, Dong Q L, Lu Q M, Lu S, Sheng Z M, Wang S and Zhang J 2017 *Phys. Plasmas* **24** 041406
[51] Law K, Bailly-Grandvaux M, Morace A, Sakata S, Matsuo K, Kojima S, Lee S, Vaisseau X, Arikawa Y, Yogo A, Kondo K, Zhang Z, Bellei C, Santos J J, Fujioka S and Azechi H 2016 *Appl. Phys. Lett.* **108** 091104
[52] Zhang J, Wang W M, Yang X H, Wu D, Ma Y Y, Jiao J L, Zhang Z, Wu F Y, Yuan X H, Li Y T and Zhu J Q 2020 *Philos. Trans. Royal Soc. A* **378** 20200015
[53] Matsuo K, Nagatomo H, Zhang Z, *et al.* 2017 *Phys. Rev. E* **95** 053204
[54] Perkins L, Logan B, Zimmerman G and Werner C 2013 *Phys. Plasmas* **20** 072708
[55] Miley G, Hora H and Kirchhoff G 2016 *J. Phys. Conf. Ser.* **717** 012095
[56] Weng S M, Zhao Q, Sheng Z M, Yu W, Luan S X, Chen M, Yu L L, Murakami M, Mori W B and Zhang J 2017 *Optica* **4** 1086
[57] Winjum B, Tsung F and Mori M 2018 *Phys. Rev. E* **98** 2018
[58] Edwards M R, Shi Y, Mikhailova J M and Fisch N J 2019 *Phys. Rev. Lett.* **123** 025001
[59] Li X C, Guo F and Liu Y H 2021 *Phys. Plasmas* **28** 052905
[60] Drake J, Opher M, Swisdak M and Chamoun J 2010 *Astrophys. J.* **709** 963
[61] Zenitani S and Hoshino M 2001 *Astrophys. J.* **562** L63